Microfluidic platform for multiplexed cell sampling and time-resolved SPR-based cytokine sensing in a rheumatoid arthritis model system

Richard Novak, PhD

February 9, 2014

Marshall Plan Scholarship – Final Report

Introduction

Over the last 5 years as a result of large strides in 3D cell culture innovation, there has been a push toward the development of organs-on-a-chip, or microfluidic systems that support the growth of functional miniature human organs.[1–4] The principal aim of these systems is the acceleration of drug testing by increasing screening efficacy. In traditional drug development, candidate compound libraries are screened for desired activity in cell lines, with further efficacy and safety studies occurring in animal models and, for the small pool of successful candidates, in a series of 3 human clinical trials. The main problem with this approach is the failure of vast numbers of compounds very late in the development process. In part, this is due to the lack of tissue and organ interactions during cell line testing, and due to animal models not being adequately representative of human disease states and drug side effects. It is also unclear how many candidates fail the screening process in animals but could still prove effective in humans. The proposed solution is to develop microscale human organs that can be linked together into a "human-on-a-chip."[5,6] This setup can then replace animal testing and accelerate drug development by providing a platform where it is possible to screen drugs for safety and efficacy in a human-like clinically-relevant setting. A number of organ systems and some connected organs have been published and significant funding is being allocated to their further development in the United States and European Union.[2,6–8] Despite the advances, less focus has been placed on analytical techniques that can be used to monitor cultures in real time. Analysis of supernatant for various metabolic and secreted protein products is critical for understanding the output of organs that may affect other systems within an individual, and this has been demonstrated for microfluidic cultures.[9] The Ertl group has demonstrated multiparameter real-time monitoring capabilities in simpler on-chip cultures, including electrical impedance and optical monitoring as well as 2D oxygen microenvironment sensing.[10–12] Yet nearly all devices so far have not incorporated robust fluid handling and multiplexing capability that would enable dynamic stimulation and analysis and leverage real-time sensing. The projects presented here are part of an ongoing collaboration between the Mathies Lab at University of California, Berkeley at the Ertl Lab at the Austrian Institute of Technology/University of Natural Resources in Vienna. These projects highlight possible paths for microfluidic device development that would provide automated culture and detailed biomolecular analysis of synthetic organ-on-chip systems.

Integrated microfluidic cell culture

To maximize the potential of microfluidic cell culture systems, additional integrated functions, including medium degassing and fluid actuation and routing, are required. These features eliminate bubble formation that is disruptive to cell and tissue layers in the confines of a microchannel, and the pumping provides a low dead volume actuator and fluid routing system for probing the effects of pulsed stimuli and drugs and for device loading and operation. As part of an ongoing collaboration with Peter Ertl's group at the Austrian Institute of Technology and the University of Natural Resources in Vienna, Austria, I incorporated a microdegasser and micropump for long-term microfluidic cell culture and robust operation.

The foundation of the microfluidic cell culture chip is a glass sensing layer composed of gold interdigitated electrodes with 5 and 20 μm pitch and passivated with a 200 nm thick SiN layer as shown in Figure 1A. It is fabricated via standard photolithography and gold deposition processes

described previously.[10] A 250 μm thick PDMS flow cell, cut with a Graphtec computer controlled cutter, defines the cell culture chamber. Electrical impedance is sensed via a custom digital signal generator and impedance sensing circuit, shown in Figure 1B, that can analyze impedance at frequencies from 10 kHz to 100 kHz. The circuit is connected to a National Instruments digital acquisition card (NI USB-8541) and communicates via an I^2C interface. The connection is facilitated via spring-loaded pins in the circuit board and held in place in an aluminum manifold that contains two circuit boards and the microfluidic device. The manifold is maintained at 37 ^oC by continuous perfusion of water from an external heated reservoir. The entire assembly is situated under an upright microscope for time lapse imaging. In initial tests, glass with drilled via holes and glued connectors was used to seal the cell culture chamber. A syringe pump was used to provide continuous perfusion of fresh medium to cells after being passed through an HPLC degasser.

A.

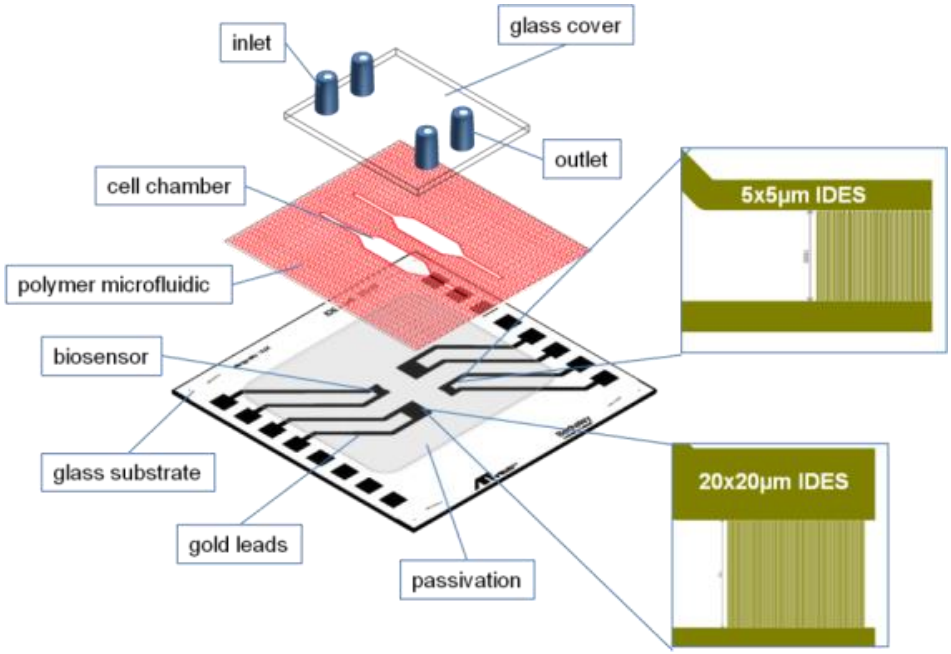

B.

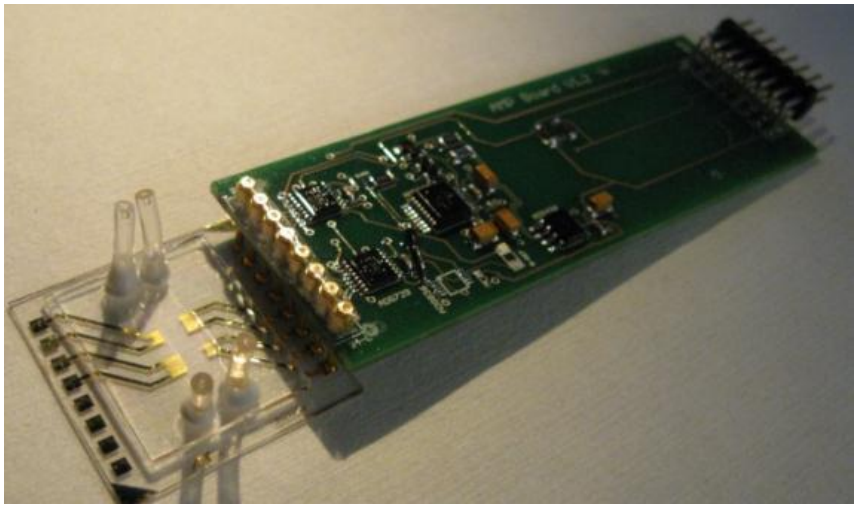

Figure 1. *(A) Diagram of interdigitated electrodes and basic flow cell fluidics for real-time electrical impedance monitoring of microfluidic cell cultures. Gold electrodes with 5 and 20 µm pitch spacing sense at different channel heights. SiN passivation eliminates DC current and provides a homogenous surface for cell adhesion following coating with fibronectin or gelatin. (B) Microfluidic cell culture with integrated interdigitated electrode sensors shown connected to a custom impedance analyzer circuit. The surrounding aluminum manifold and second circuit board are omitted for clarity. Spring-loaded pins facilitate contact with the chip pads and enable quick chip exchange. The circuit board is connected to a National Instruments digital acquisition card for power and communication.*

This simple system was used by members of the Ertl group to maintain a co-culture of human vascular endothelial cells (HUVEC) and basophils as a model of vascular response to allergens. Basophils bind IgE and release histamine in response to antigen recognition. HUVECs are endothelial cells that line blood vessel walls and increase permeability in an allergy response.[13] Figure 2 presents the data obtained from this "allergy-on-chip" model system by Ertl Lab members prior to my involvement in the project. The impedance measurement trace in Figure 2A shows the initial increase in impedance resulting from two serial HUVEC seedings. The cells were allowed to adhere and form a confluent layer over approximately 24 h. Basophils opsonized with IgE were added on top of the layer, best seen in Figure 2B, and also allowed to adhere. Due to the thickness of the HUVEC layer relative to the interdigitated electrode pitch, the top basophil layer did not significantly change the impedance sensor readout. However, the addition of antigen to the medium at 33 h resulted in a sudden decrease in impedance due to the release of histamine by the basophils causing increased HUVEC permeability. The data demonstrate the sensitivity provided by electrical impedance measurements that allow detection of subtle cellular properties not visible via microscopy.

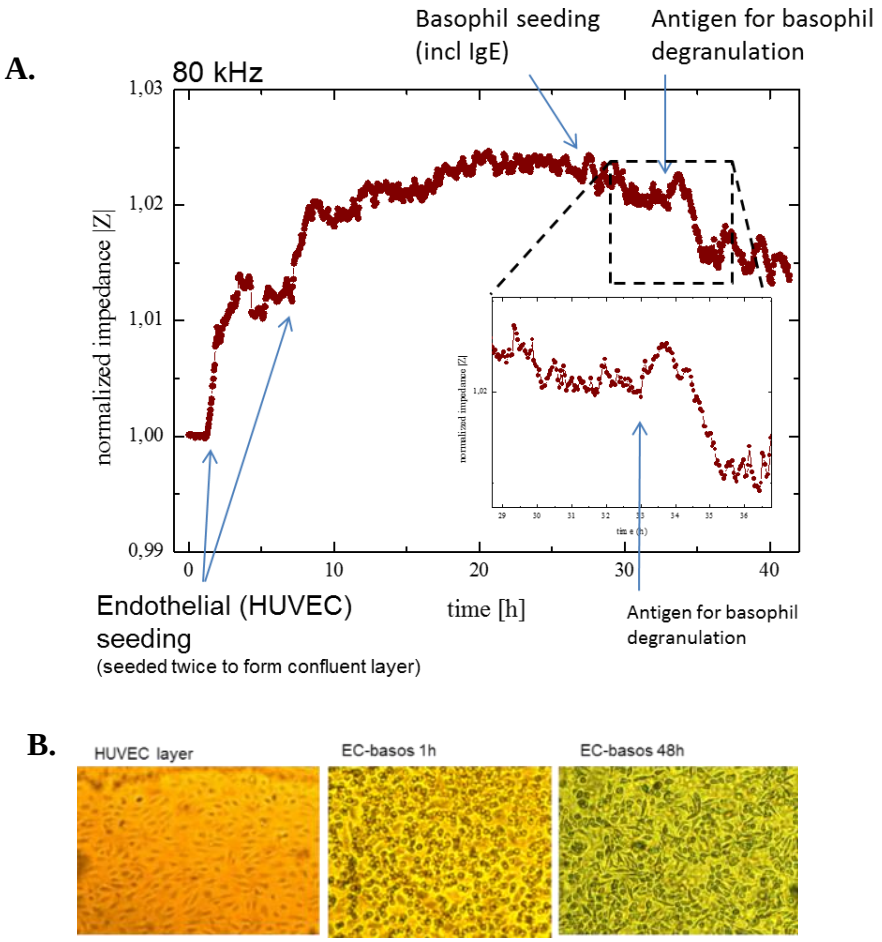

Figure 2. *HUVEC and basophil co-culture for an allergy-on-chip model system. (A) A confluent layer of HUVECs was formed by two cell seedings, mimicking the artery wall. Basophils opsonized with IgE, while beyond the IDE sensor detection range, resulted in significant impedance shifts by perturbing the confluent endothelial cell layer following degranulation and histamine release. (B) Photographs demonstrate successful co-culture of confluent HUVEC layer with overlaid basophils that is stable for at least 2 days of culture.*

This initial syringe pump-based setup limited usability and resulted in noisy electrical impedance data due to solution exchange causing cells to physically shift on the substrate. In addition, the commercial degasser dead volume not only required large culture medium volume but also eliminated the possibility to test short pulses of stimuli due to Taylor dispersion in the long degassing coils. The solution was to integrate pumping and degassing into a single device with the footprint matching that of the existing sensing chip and flow cell. Using rapid prototyping I developed at UC Berkeley,[14] we fabricated the device shown in Figures 10.3 and 10.4 from cycloolefin copolymer, which offered excellent biocompatibility and optical transparency. Figure 3 shows an exploded view of the device layers, highlighting the microfluidic components that provide medium actuation and enable cell loading, pneumatic controls and degassing, and the PDMS flow cell for cell culture. The degasser consists of a sinusoidal channel with a superimposed ladder-like pneumatic structure separated by a thin PDMS membrane. Since PDMS is gas permeable, a constant vacuum provides sufficient degassing to prevent bubble formation inside the device. The glass sensing layer forms the bottom of the cell culture chamber. The assembled device, shown as a diagram in Figure 4A and photographed in Figure 4B, occupies the space above the flow cell and sensor area, fitting into the existing manifold.

The micropump provides continuous perfusion to cells with minimal dead volume (~10 μL) while reversing the flow enables highly efficient loading of cells via the outlet. The micropump is controlled via a custom pneumatic control box, shown in Figure 5A. The control box is designed to be a portable standalone system for long-term use that only requires AC power, a vacuum source, and pressurized air. An Arduino processor and onboard memory controls a bank of three-way solenoid valves, described in greater detail in earlier chapters and published work.[15,16] Tubing connects the control box with the integrated device manifold. Regulated nitrogen and vacuum lines input the control box and are routed to the microfluidic device according to an uploaded program. By selecting actuation pressures and times, a broad range of flow rates (5-35 μL/min) can be achieved with the microfluidic design used here, as presented in Figure 5B. Cell cultures were maintained in excess of 7 days without bubble formation or loss of cell viability. The fully integrated approach offers a high degree of dosing precision, as each pump stoke contains a well-defined bolus of fluid, which can be used for metering of drugs or stimuli. In future design iterations, the device can incorporate additional fluidic inputs for automated reagent exchange, staining, and stimulation.

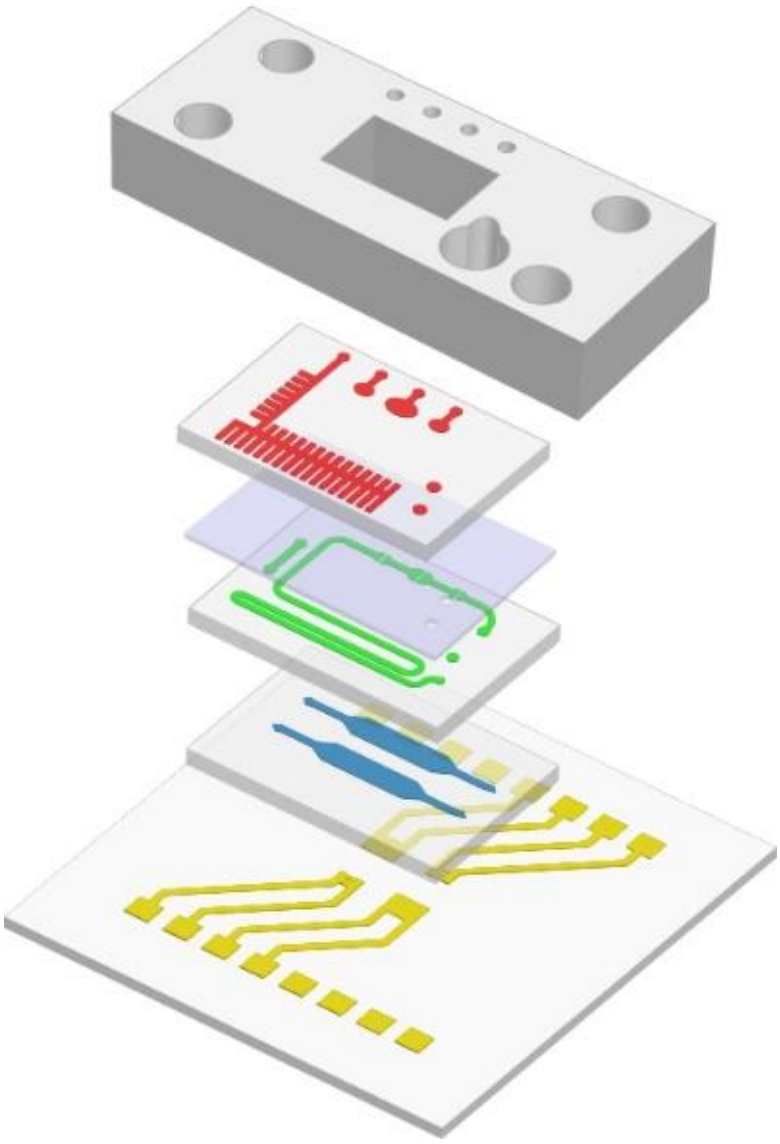

Figure 3. *Exploded view of five-layer integrated microfluidic cell culture and analysis system showing impedance sensing IDES layer (gold), cell culture chambers (blue), microfluidic channels (green) separated by a thin PDMS sheet from the pneumatic control and degassing layer (red), and an aluminum manifold for ease of assembly and operation (gray).*

A.

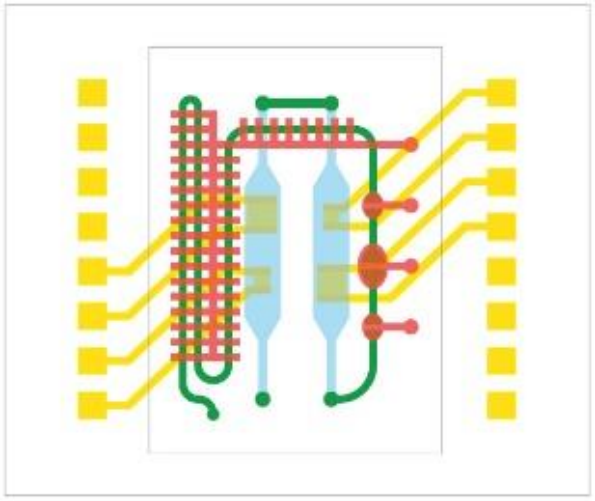

B.

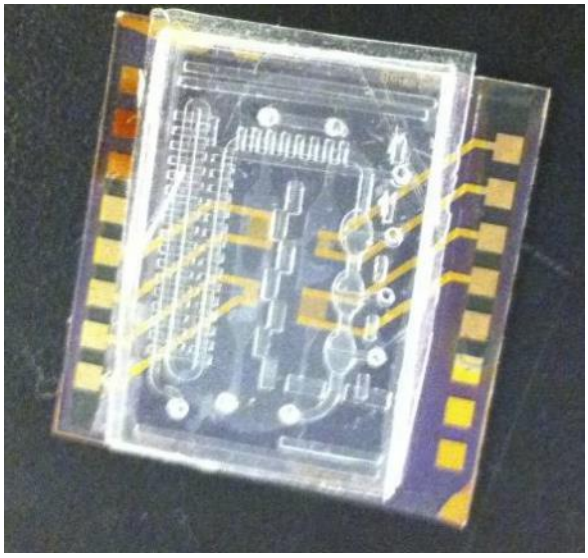

Figure 4. *Assembled integrated microfluidic cell culture device (A) diagram and (B) photograph, showing the arrangement of microvalves for fluid actuation, an extended degassing region for bubble-free cell culture, and interdigitated electrodes for continuous non-invasive cell monitoring.*

A.

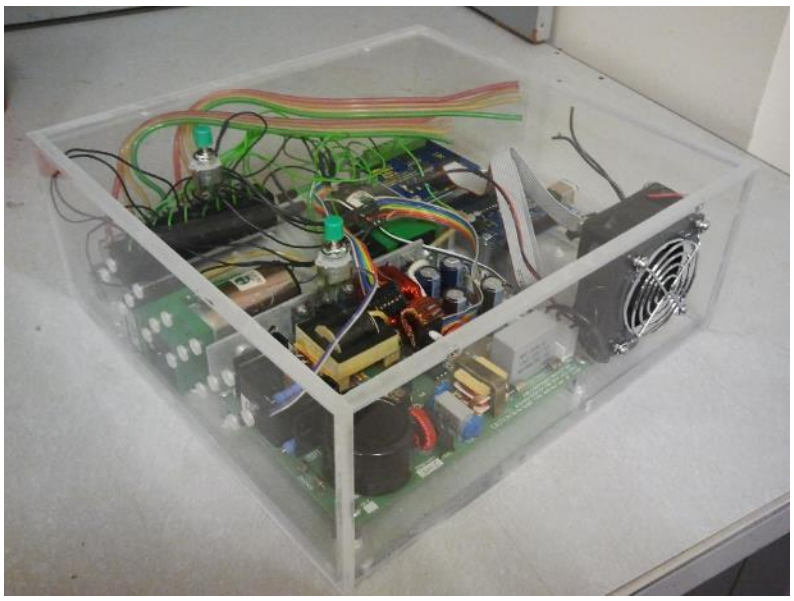

B.

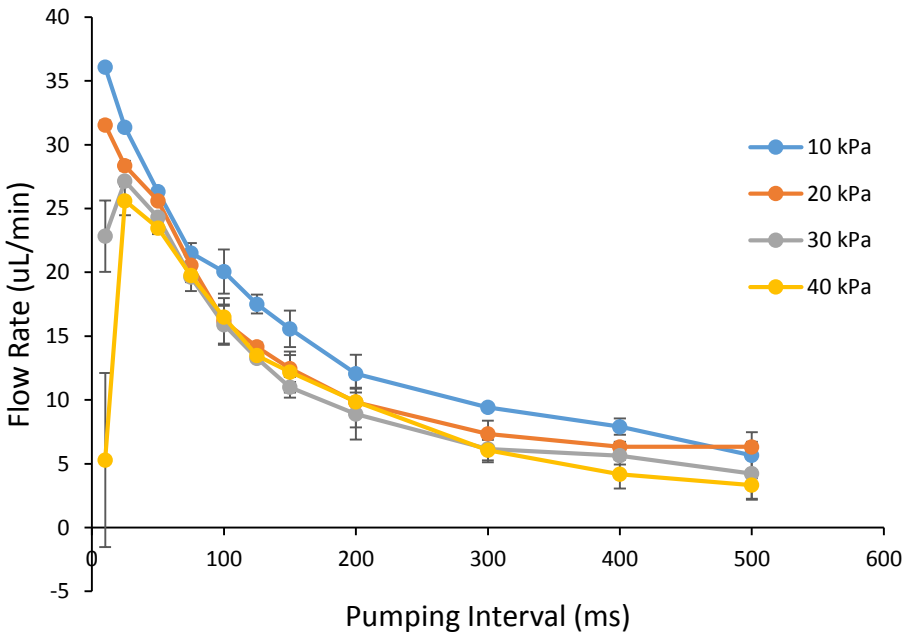

Figure 5. *(A) Photograph of the standalone pneumatic control box used to control micropumps for cell loading and perfusion. Buttons in the lid select the pump sequence to be run. (B) Plot showing flow rate in μL/min as a function of pumping interval between each pump step at the specified actuation pressures. Vacuum was maintained at -40 kPa throughout.*

Time-resolved immunoassay of microculture medium

Analyzing secreted metabolites and proteins is an attractive means of monitoring organs-on-chip and other cultures with very small cell numbers, enabling assessment of inflammation and metabolic status.[9,17] It can provide the information needed to connect single cell-level phenotypes with population-level behavior. The addition of highly multiplexed real-time measurement of the secretome would add to our understanding of organ model systems.

The scale of microfluidic systems combined with constant perfusion of fresh medium are a double edged sword. On the one hand, organs-on-chip provide the capability to perform dynamic studies of cellular response. For example, pulsed doses can be delivered and removed with very high time resolution and with predictable changes in local concentration due to diffusion. On the other hand, microfluidic systems simply do not produce amounts of secreted protein or metabolites sufficient for traditional bulk scale assays. Collecting large volumes of culture medium can overcome the lack of analyte, but this then prevents dynamic studies of cell behavior that is necessary to observe in real-time or near real-time. This technological barrier must be overcome to enable sensitive analysis of organ-on-chip secretomes.

As part of the Marshal Plan Scholarship, I worked in the Ertl group to devise a way to measure secreted interleukin 6 (IL-6) inflammatory cytokine from stimulated fibroblasts with very high time resolution. Figure 6 presents the microfluidic processor for multiplexed, time-resolved immunoassays. The device allows 6 samples to be serially monitored by a single sensor functionalized with anti-IL-6 capture antibodies.

The microfluidic device was fabricated using the optimized nickel mold fabrication and hot embossing protocol described in Chapter 4, with the final device embossed into 1 mm-thick polycarbonate sheets. A 250 μm-thick PDMS membrane sandwiched between the fluidic and pneumatic layers provides valving and pumping capability. Bus valves, best seen in Figure 6A, allow liquid to pass through the main fluidic channel even when valves to other inputs are closed. As in the integrated micropump-actuated cell culture system, a custom pneumatic control box shown in Figure 6C controls on-chip pumping and reagent selection through microvalve regulation. The compact form factor enables the microfluidic device to be set up in various SPR systems and easily resituated.

Figure 7 presents the experimental setup for initial time-resolved immunoassay characterization. The sensor consists of a sheet of glass with a 45 nm evaporated gold layer that is functionalized with a biotinylated thiol self-assembled monolayer, followed by streptavidin and, later, biotinylated anti-IL-6 capture antibodies. The glass is coupled to a prism in a standard Kretchmann configuration. A 633 nm laser beam is used for illumination. The beam is passed through a 1 kHz beam chopper and detected by the SPR CCD detector using a lock-in amplifier to remove extraneous signals, including ambient light. The SPR setup is mounted on a computer-controlled dual stepper motor gantry that enables accurate angular positioning. Fluidic coupling is achieved by a Teflon and glass flow cell, approximately 9 mm by 15 mm and 100 μm high. The microfluidic device programmatically selects sample inputs and reagents and pumps them via the integrated micropump through the flow cell.

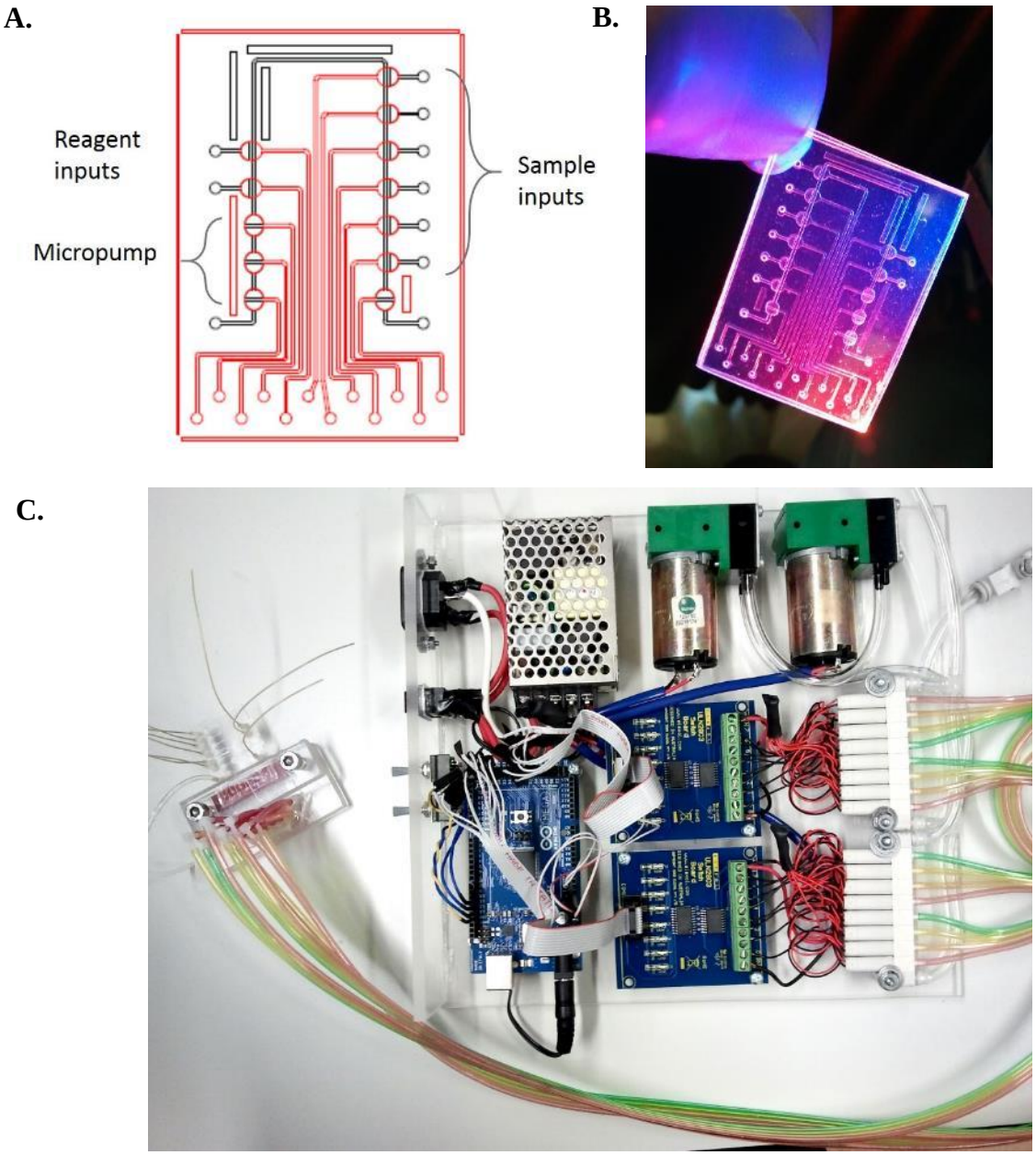

Figure 6. *Microfluidic processor for time-resolved immunoassays. (A) Diagram of microfluidic design for routing 6 samples to a sensor and providing supporting reagents for washing between samples, labeling with fluorescent secondary antibody, and regenerating sensor surface. The pneumatic lines (red) control PDMS membrane valves along the fluidic line (black), enabling fully automated immunoassays through programmable valving and integrated pumping. (B) Photograph of assembled device fabricated from polycarbonate using rapid prototyping via hot embossing. (C) Custom pneumatic control box for portable microfluidic control of pumping and fluid routing connected to the microfluidic device in a manifold on the left. An Arduino processor enables complex programs to be uploaded and run by toggling control buttons.*

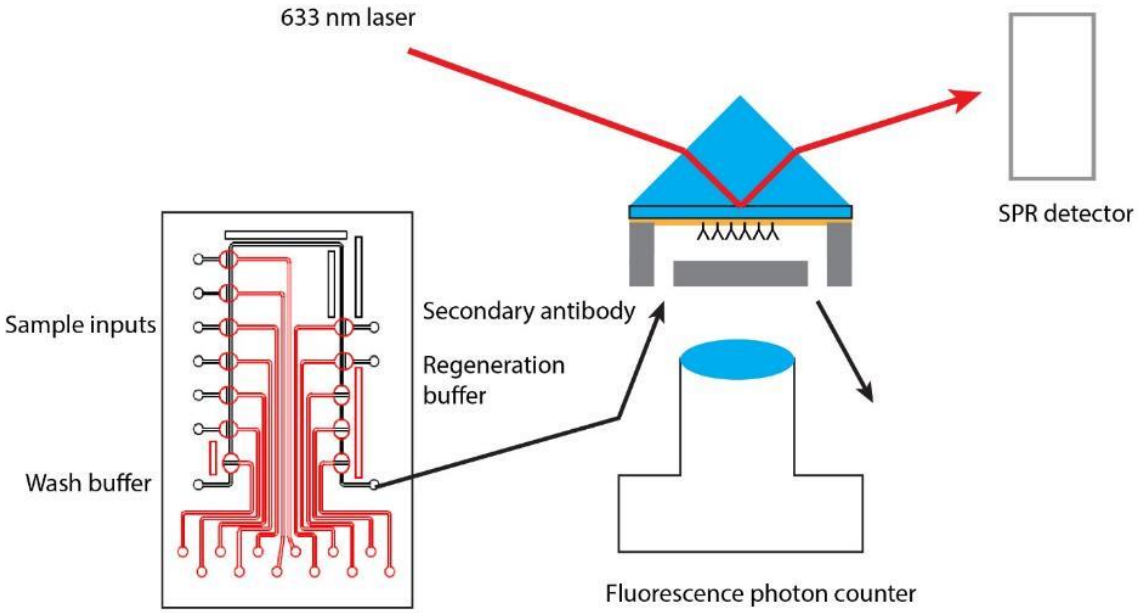

Figure 7. *Diagram of time-resolved immunoassay experimental layout. The microfluidic processor on the left controls reagent selection and provides fluid actuation through an integrated micropump. Inputs are sampled serially for a capacity of 6 independent samples using this device. All fluid is pumped through the SPR sensor flow cell via PEEK tubing. The sensor consists of a glass prism coupled to a gold-coated glass plate functionalized with anti-IL-6 capture antibodies. A 633 nm laser passing through the prism and into the SPR detector is used to detect refractive index changes due to protein capture. In parallel, the laser beam provides excitation for Alexa 647-labeled secondary antibodies whose fluorescence is sensed by the photon counter.*

The microfluidic system automatically conducted cyclic immunoassays, including sensor flushing, sampling of analytes, further washing, labeling with Alexa 647-labeled anti-IL-6 secondary antibody in a sandwich assay format, washing off excess secondary label, followed by sensor regeneration with glycine buffer pH 1.5. Figure 8A presents fluorescence and SPR measurements over time as a 100 ng/mL IL-6 sample is repeatedly assayed via different inputs. Not only do repeat fluorescence measurements exhibit high reproducibility, but the trace indicates successful sensor regeneration without loss of sensor specificity or sensitivity. Indeed, we were able to regenerate the sensor more than 50 times with no discernible deterioration. The SPR signal, however, could not detect IL-6 binding below 100 ng/mL even after secondary antibody labeling. As a result, we opted to utilize the fluorescence readout for greater sensitivity. The SPR flow cell fluidic resistance proved to be a significant obstacle to robust micropumping in the current chip design. We incorporated an inline peristaltic pump to replace the onboard micropump for the remainder of the experiments, though this could be solved by integrating SPR and fluorescence measurements with the chip. Figure 8B shows three overlapping fluorescence traces over time during fully automated standard curve generation. The highly reproducible fluid handling enabled generation of the standard curve in Figure 8C with a limit of detection between 10 and 100 pg/mL, comparing favorably to the 10 pg/mL limit of detection for the antibody set used. Note that full analysis of 6 samples, complete with sensor regeneration, required less than 90 min.

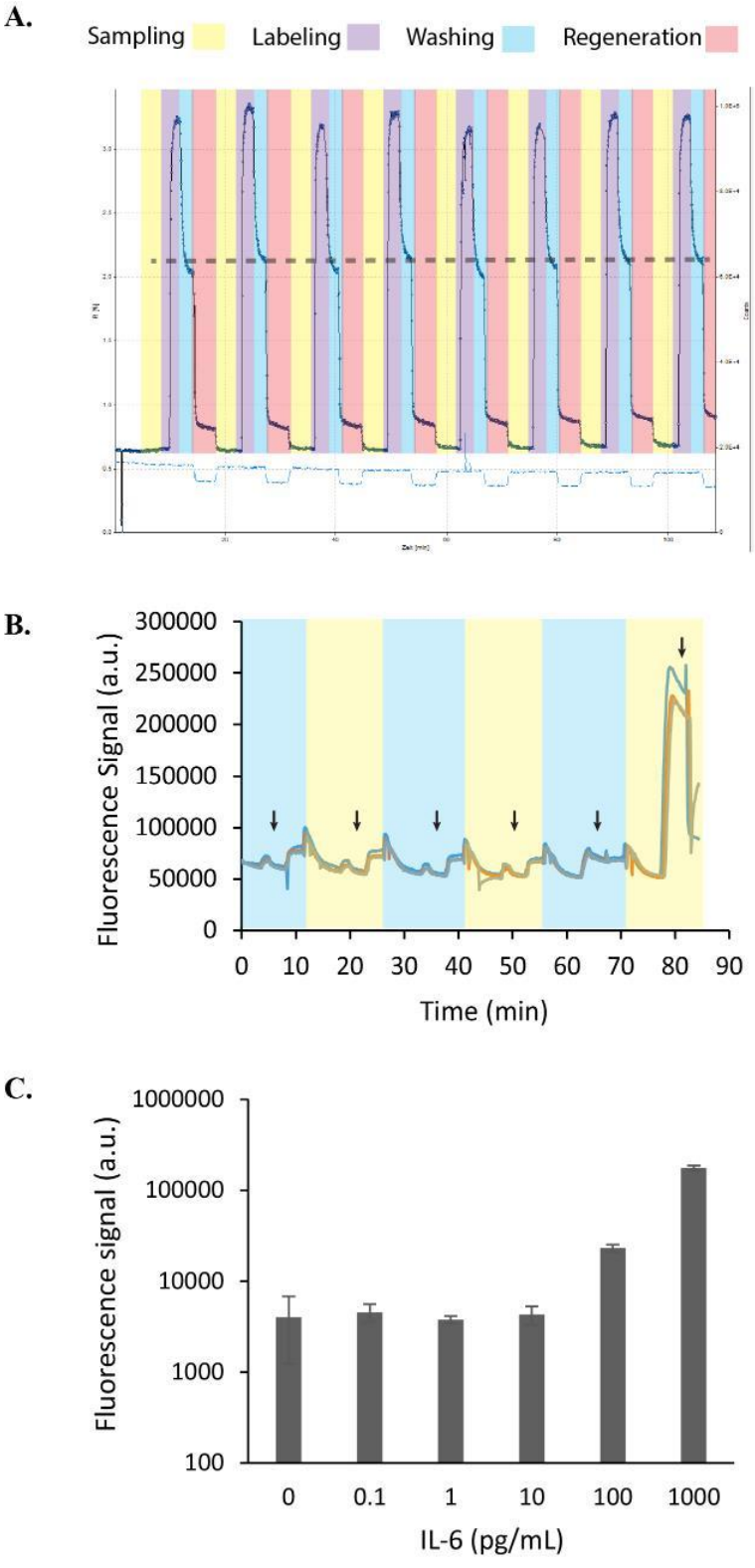

Figure 8. *Automated microfluidic IL-6 immunoassay results. (A) Time trace of SPR (dotted light blue line) and fluorescence (solid dark blue line) signals during a fully automated repeated*

analysis of a 100 ng/mL IL-6 sample in buffer. Color shading highlights specific assay states. The dashed gray line is a visual guide showing the approximate assay readout for each sample, demonstrating high reproducibility across 8 samples. The SPR signal changes significantly only during sensor regeneration. (B) Time trace of fluorescence signal during three repeats of a negative control and five increasing 10-fold IL-6 dilutions, with each sample distinguished by a change in shading. Arrows indicate fluorescence measurement points taken after washing off excess labeling antibody. Excellent run-to-run reproducibility can be observed. (C) Standard curve of IL-6 detection based on fluorescence obtained using the fully automated setup. Limit of detection lies between 10 and 100 pg/mL.

Integrated organ-on-chip analytical platform

Given the several pitfalls observed during the development of the time-resolved immunoassay system, a second generation platform that not only overcomes the technical barriers but adds greater multiplexing capability and portability is presented in Figure 9. The proposed design integrates earlier microfluidic cell culture designs with multiparameter analysis of both the organ cultures as well as secreted products. The underlying design is based on the microfluidic layout used for time-resolved immunoassay development. A single micropump at the outlet actuates all fluidic components, including cell culture perfusion. Six culture chambers can be maintained and assayed in parallel. Upstream of each chamber, additional microvalves could be added to provide high time resolution dosing capability. Each chamber is addressed serially, and a defined volume of medium is pumped across the sensor, thus replacing medium in the cell chambers. Adequate medium exchange is possible due to rapid fluid actuation stemming from a fully integrated all-microfluidic system. Capture antibodies for several proteins are patterned in the sensing region to not only provide greater multiplexing capability but also concentrate the analytes for greater sensitivity. Multiplexed capture antibodies also provide a convenient internal control. Following analyte capture, secondary antibodies labeled with a single fluorophore are flowed into the chamber, providing a label for epifluorescence imaging and subsequent image analysis and target quantitation. Epifluorescence imaging is preferable to SPR analysis as it is readily multiplexed and can be built in a compact and portable form factor for bench-top analysis.

This integrated organ-on-chip analytical platform provides the capabilities and scalability needed for basic investigations into the role of cell heterogeneity in tissue and organ behavior as well as for more rapid and effective drug screening. The platform allows additional expansion of analytical modes, such as through the addition of mass spectroscopy to the outlet for metabolite monitoring or the addition of digital RT-PCR for measurement of secreted RNA. Single cell analysis can be further enhanced by the addition of sophisticated microscopy techniques, such as Raman microscopy and end-point single cell transcriptome analysis *in situ*,[18,19] since most organ-on-chip devices are conveniently planar.[2] Alternatively, single cell genetic analysis can be performed in droplets as described in earlier chapters if cells are released from the culture chambers. The application of massively multiplexed multiparameter assays to single cells and organ-level interactions will undoubtedly provide a wealth of data for understanding fundamental cellular biology mechanisms, provide novel targets for therapy, more effectively screen drug libraries, and better guide clinical decisions.

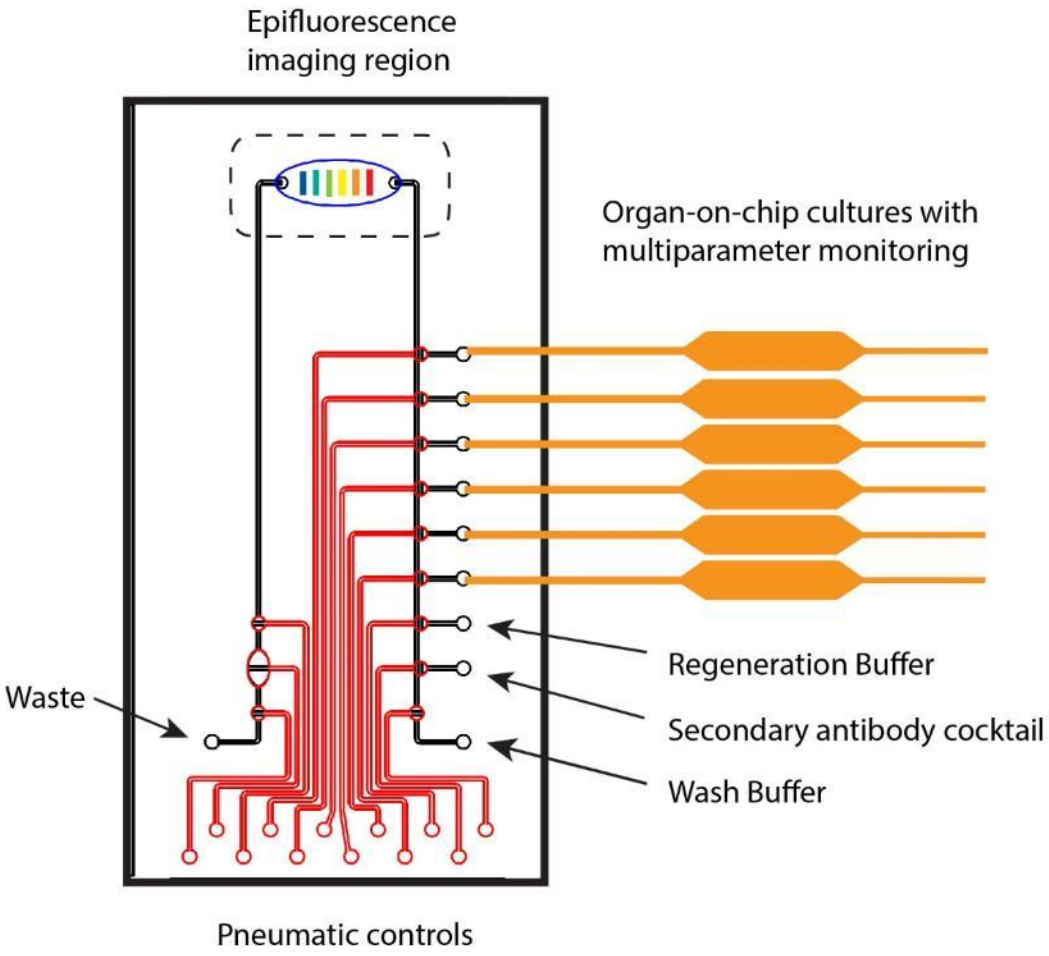

Figure 9. *Proposed second generation time-resolved immunoassay multiplexed for 6 organs-on-a-chip and 6 protein targets. The microfluidic device shares many attributes of the initial design, but this system implements immunofluorescence imaging in an integrated sensing region with patterned capture antibodies against 6, and probably more, protein targets represented here by the multicolored bars. Patterning capture antibodies will also increase sensitivity by concentrating the signal to a smaller area. The low fluidic resistance system facilitates robust pumping and fast reagent exchange for low assay times. Organs-on-chip are connected directly to the sample input ports, and rapid serial sampling of medium provides culture perfusion. Each organ-on-chip culture is also monitored in real time as demonstrated previously.*

Development of hot embossing capability at AIT

Given the need to quickly modify microfluidic designs in order to optimize pumping and adjust channel and chamber geometries, I designed a second generation hot embossing machine (Figure 10) that I built along with members of the Ertl Lab. While identical in function to the Berkeley machine, this device offers greater ease of use and faster operation.

Figure 10. *Hot embosser built for the Ertl Lab, shown after assembly (left) and closeup view of the temperature controller and heated platens (right). The frame consists of a 20 ton hydraulic press with heated platens. Temperature is regulated by two independent heaters and temperature controllers (gray box attached to press).*

Temperature control is achieved through off-the-shelf components wired to facilitate temperature feedback for each platen independently. Figure 11 shows the electrical circuit.

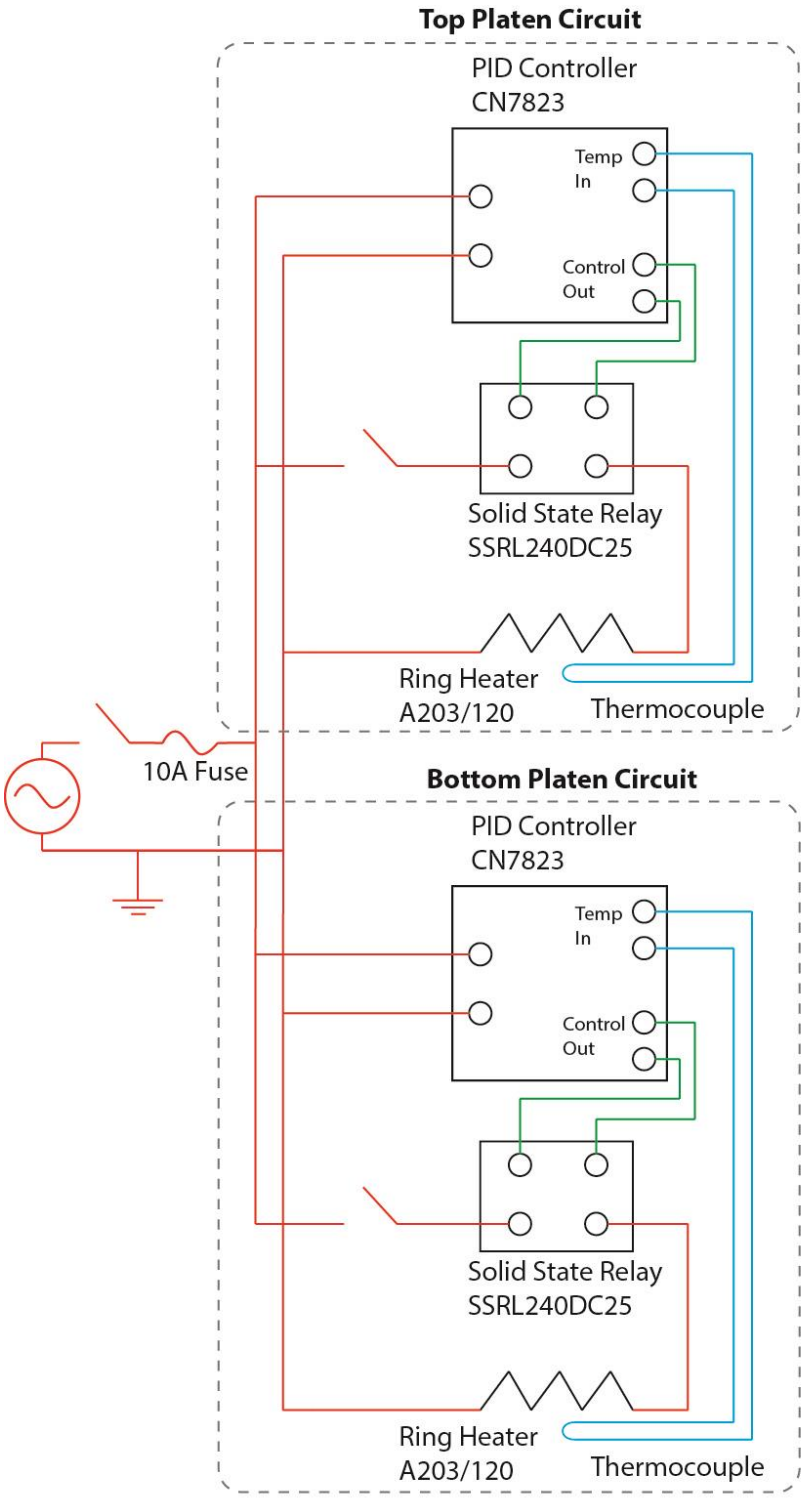

Figure 11. *Temperature control feedback circuit implemented in the second generation hot embossing machine built at AIT.*

The hot embosser will now enable rapid prototyping of microfluidic devices and possibly peripherals like cartridges within the lab environment. Since hot embossing, particularly if coupled with a fast mold fabrication method, allows for a rapid design validation turnaround, faster progress can be made on research projects. For example, chips with a particular design can be fabricated in the morning, tested by the afternoon, and a second revision can be implemented by the next day. Compared to most current iteration timelines of days to weeks, this can have a profound impact on accelerating the pace of microfluidic research. Finally, all prototyping can take place using commercially-viable materials and processes that will improve chances for success if a microfluidic solution is to be commercialized.

Summary

The Marshall Plan Scholarship has furthered collaboration between UC Berkeley and the Austrian Institute of Technology/University of Natural Resources in Vienna. Thanks to the funding, I was able to continue working with the Ertl Lab on the development of microfluidic systems for organ-on-chip culture and analysis. In Vienna, I was particularly focused on establishing an automated immunoassay for IL-6 in order to understand upregulation of this cytokine in response to antigen exposure. The initial experiments proved successful, though additional design changes are needed. As a result, I constructed a hot embossing machine to facilitate rapid design iteration of microfluidic circuits. This project has excellent potential to produce novel scientific findings related to inflammation response as well as build a technology foundation for assaying organ-on-chip cultures with unprecedented detail.

References

(1) Domansky, K.; Inman, W.; Serdy, J.; Dash, A.; Lim, M. H. M.; Griffith, L. G. *Lab. Chip* **2010**, *10*, 51–58.

(2) Huh, D.; Matthews, B. D.; Mammoto, A.; Montoya-Zavala, M.; Hsin, H. Y.; Ingber, D. E. *Science* **2010**, *328*, 1662–1668.

(3) Schimek, K.; Busek, M.; Brincker, S.; Groth, B.; Hoffmann, S.; Lauster, R.; Lindner, G.; Lorenz, A.; Menzel, U.; Sonntag, F.; Walles, H.; Marx, U.; Horland, R. *Lab. Chip* **2013**, *13*, 3588–3598.

(4) Sonntag, F.; Schilling, N.; Mader, K.; Gruchow, M.; Klotzbach, U.; Lindner, G.; Horland, R.; Wagner, I.; Lauster, R.; Howitz, S.; Hoffmann, S.; Marx, U. *J. Biotechnol.* **2010**, *148*, 70–75.

(5) Chan, C. Y.; Huang, P.-H.; Guo, F.; Ding, X.; Kapur, V.; Mai, J. D.; Yuen, P. K.; Huang, T. J. *Lab. Chip* **2013**, *13*, 4697.

(6) Huh, D.; Hamilton, G. A.; Ingber, D. E. *Trends Cell Biol.* **2011**, *21*, 745–754.

(7) Ghaemmaghami, A. M.; Hancock, M. J.; Harrington, H.; Kaji, H.; Khademhosseini, A. *Drug Discov. Today* **2012**, *17*, 173–181.

(8) Moraes, C.; Mehta, G.; Lesher-Perez, S. C.; Takayama, S. *Ann. Biomed. Eng.* **2012**, *40*, 1211–1227.

(9) Shintu, L.; Baudoin, R.; Navratil, V.; Prot, J.-M.; Pontoizeau, C.; Defernez, M.; Blaise, B. J.; Domange, C.; Péry, A. R.; Toulhoat, P.; Legallais, C.; Brochot, C.; Leclerc, E.; Dumas, M.-E. *Anal. Chem.* **2012**, *84*, 1840–1848.

(10) Charwat, V.; Purtscher, M.; Tedde, S. F.; Hayden, O.; Ertl, P. *Lab. Chip* **2013**, *13*, 785–797.

(11) Gottschamel, J.; Richter, L.; Mak, A.; Jungreuthmayer, C.; Birnbaumer, G.; Milnera, M.; Brückl, H.; Ertl, P. *Anal. Chem.* **2009**, *81*, 8503–8512.

(12) Ungerböck, B.; Charwat, V.; Ertl, P.; Mayr, T. *Lab. Chip* **2013**, *13*, 1593–1601.

(13) Ehringer, W. D.; Edwards, M. J.; Miller, F. N. *J. Cell. Physiol.* **1996**, *167*, 562–569.

(14) Novak, R.; Ranu, N.; Mathies, R. A. *Lab. Chip* **2013**, *13*, 1468–1471.

(15) Zeng, Y.; Novak, R.; Shuga, J.; Smith, M. T.; Mathies, R. A. *Anal Chem* **2010**, *82*, 3183–3190.

(16) Shuga, J.; Zeng, Y.; Novak, R.; Lan, Q.; Tang, X.; Rothman, N.; Vermeulen, R.; Li, L.; Hubbard, A.; Zhang, L.; Mathies, R. A.; Smith, M. T. *Nucleic Acids Res.* **2013**, *41*, e159–e159.

(17) Satoh, W.; Takahashi, S.; Sassa, F.; Fukuda, J.; Suzuki, H. *Lab. Chip* **2009**, *9*, 35–37.

(18) Freudiger, C. W.; Min, W.; Saar, B. G.; Lu, S.; Holtom, G. R.; He, C.; Tsai, J. C.; Kang, J. X.; Xie, X. S. *Science* **2008**, *322*, 1857–1861.

(19) Larsson, C.; Grundberg, I.; Söderberg, O.; Nilsson, M. *Nat. Methods* **2010**, *7*, 395–397.